

Comparative Studies on the Properties of New and Conventional Perovskite-Type $LaCoO_3$

Lin Huang,* Mahbod Bassir, Echchahed Bousselham, and Serge Kaliaguine

Department of Chemical Engineering, Laval University, Ste-Foy, Quebec, Canada G1k 7P4

Received July 7, 2004; E-mail: huanglin1@yahoo.com

The physical properties and redox chemistry of perovskite-type $LaCoO_3$ prepared by reactive grinding and by the citrate method, have been comparatively studied by temperature-programmed reduction (TPR), X-ray diffraction (XRD), N_2 adsorption–desorption, and infrared spectroscopy (IR). XRD and N_2 adsorption–desorption measurements show that $LaCoO_3$ prepared by reactive grinding possesses a smaller particle size and thus a greater specific surface area. An IR study suggests that there would exist a large amount of oxygen defects in $LaCoO_3$ prepared by reactive grinding. TPR results illustrate that the reduction of $LaCoO_3$ to Co^0/La_2O_3 requires a higher temperature for a sample prepared by reactive grinding than for the one prepared by the citrate method. Due to a more difficult reduction, $LaCoO_3$ prepared by reactive grinding displays a better stability of the perovskite structure than $LaCoO_3$ prepared by the citrate method under a reducing atmosphere.

Perovskite-type oxides are of interest in applied fields of physics and chemistry because of important physical characteristics such as ferroelectricity, magnetism, high-temperature superconductivity, and electro-optic effects. Transition metal-containing perovskite-type oxides have found potential catalytic applications in both the oxidation and reduction of significance over more than two decades.[1–12] $LaCoO_3$ is one of the typical mixed oxides of this family with a rhombohedral distortion of the cubic perovskite lattice. The deformation in structure may result in large changes in the electronic and chemical properties. Therefore, $LaCoO_3$ has been extensively studied and exploited as catalyst precursors for the combustion of hydrocarbons and volatile organic compounds,[2,6,8,10–14] DeNOx,[3–5,7] the electrochemical reduction of oxygen,[9] and the hydrogenation and hydrogenolysis of hydrocarbons.[2,15–21] Nevertheless, like other perovskite-type materials, the uses of $LaCoO_3$ as catalyst precursors are limited by its low specific surface area. Conventional methods for preparing perovskite-type materials involve a high-temperature calcination step, which leads to a severe sintering of crystals producing a large particle size and thus a low specific surface area. The so-called "citrate method", by which the bottom calcination temperature at 500–600 °C is adopted,[22,23] yields crystalline $LaCoO_3$ with a specific surface area as low as around 8 m^2/g only.[10]

To overcome the disadvantage of conventional preparative methods, we recently developed a reactive grinding technique allowing for the preparation of perovskite-type materials having high specific surface areas and nanosized particles.[24,25] Owing to the low grinding temperature (below 40 °C), a high specific surface area of 100 m^2/g can be reached with the aid of grinding additives. The new method has the advantages of providing a high density of active sites for catalytic reactions and lowering the preparative cost of perovskite-type materials. Cobalt-containing perovskites prepared by reactive grinding have been found to possess high catalytic activity for the oxidation of hydrocarbons.[10,11] The good catalytic performance is correlated to both a high specific surface area and a high defect density created by reactive grinding.[10,11]

In the light of the preliminary results on the physical and catalytic properties of new perovskites, we took stronger interest in exploring the surface chemistry and structural properties of new perovskites by comparing with those of conventional perovskites. We attempted to understand the discrepances in the microstructural feature between new and conventional perovskites in association with their apparent differences in particle size and specific surface area. We paid special attention to studying the redox behavior and structural stability under reducing atmospheres of new and conventional perovskites, in order that we could predict the performances and advantages of new perovskites when applied to catalytic hydrogenation.

This paper reports on comparative characterization results of new and conventional $LaCoO_3$ perovskites by TPR, XRD, and IR. Different spectroscopic characteristics and reduction behaviors are demonstrated. These results reveal the difference in the structural stability between the two $LaCoO_3$ perovskites under reducing conditions due to different preparation methods.

Experimental

Conventional $LaCoO_3$ was prepared according to the citrate method.[23] 10 g of $La(NO_3)_3 \cdot 6H_2O$ (99.99%), 6.72 g of $Co(NO_3)_2 \cdot 6H_2O$ (98+%), and 10 g of citric acid were each dissolved in 20 mL of distilled water. The solutions were then mixed together and the water was evaporated at 80 °C until a viscous liquid was obtained. This liquid was treated under a vacuum at 70 °C for 12 h. The resulting solid was calcined at 600 °C for 12 h, which gave rise to a specific surface area of 7.8 m^2/g. New $LaCoO_3$ was prepared from La_2O_3 and Co_3O_4 via reactive grinding as described previously by us.[25] La_2O_3 (99.99%) was first calcined at 600 °C for 24 h to transform any lanthanum hydroxide to lanthanum oxide. Then a mixture of La_2O_3 and Co_3O_4 (97.49%) at an atomic ratio of La/Co = 1 was introduced into a vial with three balls.

Published on the web August 4, 2005; DOI 10.1246/bcsj.78.1450

The vial and balls were made of tungsten carbide. The high-energy ball milling was processed at actual temperatures kept below 40 °C. ZnO and NaCl were used as post-treatment additives to enhance the specific surface area of $LaCoO_3$. After completion of ball milling, ZnO was leached out of the sample with a 2 M solution of NH_4Cl and NaCl was eliminated with distilled water. Residual Zn and Na were less than 0.3% and 0.001%, respectively. The resultant sample was dried in an oven at 120 °C overnight. In the final conventional and new $LaCoO_3$ perovskites, the atomic ratios of La to Co were 1.0.

TPR was carried out on a multifunctional catalyst testing and characterization apparatus RXM-100 designed by Advanced Scientific Designs, Inc. The apparatus was equipped with a quadrupole mass spectrometer UTI100 and a thermal conductivity detector (TCD). Prior to a TPR run, a sample of 100 mg was subjected to 2 h of calcination in flowing 20% O_2/He (30 mL/min) at the desired temperature, followed by 1 h of evacuation under a vacuum at the calcination temperature. A TPR profile was obtained by passing 5% H_2/Ar at the desired flow rate through the sample which was heated from ambient temperature using a desired temperature program. The effluent gas was passed through a dry ice/ethanol trap (~−75 °C) placed before TCD to remove water from the exit stream. H_2, Ar, 5% H_2/Ar, and He had a purity of 99.999%. The amount of H_2 consumed during a TPR could be obtained by integrating the TPR profile area. The reduction degree of the sample could be calculated accordingly.

XRD was performed on a PHILIPS or SIEMENS D5000 diffractometer to determine the crystal structures of powdered samples. Cu Kα radiation was used ($\lambda = 1.5406$ Å). XRD spectra were recorded with step scans from 20 to 80° in 2θ angle.

IR spectra were measured on a Nicolet MAGNA-760 spectrometer in the 700–50 cm^{-1} region at a resolution of 4 cm^{-1}. Powdered samples were supported on a polyethylene film card, a ST-IR Card purchased from Thermo Electron Corp.

N_2 adsorption–desorption measurements were undertaken on an OMNISORB100 analyzer to determine the BET specific surface areas of samples.

Elementary analyses of La, Co, Na, and Zn were performed by atomic absorption spectroscopy on a Perkin-Elmer 1100B spectrometer.

Results and Discussion

Figures 1, 2, 3, 4, and 5 show comparative XRD patterns, IR spectra, and TPR profiles of new and conventional $LaCoO_3$. The XRD spectra of new $LaCoO_3$ (Fig. 1) are consistent with those of conventional $LaCoO_3$ (Fig. 2). Note that small peaks

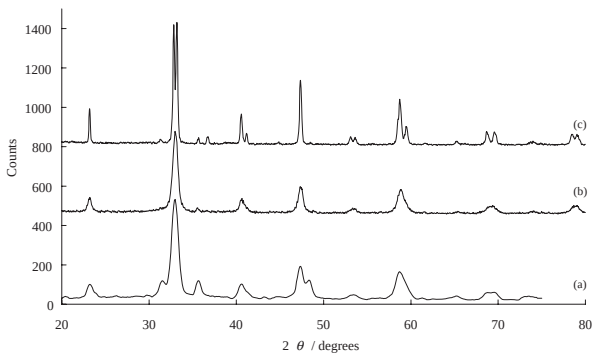

Fig. 1. XRD patterns of new $LaCoO_3$ calcined at (a) 120 °C (77.9 m^2/g); (b) 500 °C; (c) 800 °C.

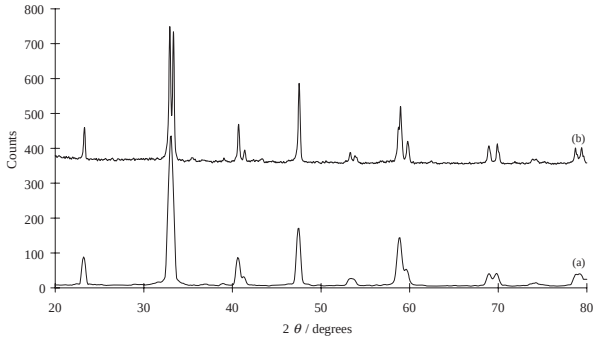

Fig. 2. XRD patterns of conventional $LaCoO_3$ calcined at (a) 600 °C (7.8 m^2/g); (b) 950 °C.

Table 1. Particle and Surface Characteristics of $LaCoO_3$

$LaCoO_3$	Calcination temperature/°C	Particle diameter[a)]/nm	BET surface area/$m^2\ g^{-1}$
New	120	10.5	77.9
New	500	17.0	56.1
New	800	42.0	32.7
Conventional	600	17.0	7.8
Conventional	950	38.1	—

a) Estimated in terms of Sherrer formula.

appearing at 31.8, 35.8, and 48.5° in Fig. 1 are assigned to trace amounts of tungsten carbide, ball milling material, which is slightly mixed to new $LaCoO_3$ after reactive grinding. It can be seen from Figs. 1 and 2 that the peak width of new $LaCoO_3$ calcined at 120 °C is indeed larger than those of $LaCoO_3$ calcined at higher temperatures, indicating that the former possesses a smaller particle size than the latter. In the cases with smaller particle sizes, two broad peaks at around 32.9 and 33.3° result in one superimposing peak at around 33.1° (Figs. 1(a), (b), and Fig. 2(a)). In Table 1 are listed the particle and surface parameters of some studied $LaCoO_3$ materials. The particle size does increase with increasing calcination temperature of $LaCoO_3$. It was estimated by the Sherrer method that the mean particle diameters of new $LaCoO_3$ after calcination at 120, 500, and 800 °C were 10.5, 17.0, and 42.0 nm, respectively and those of conventional $LaCoO_3$ after calcination at 600 and 950 °C were 17.0 and 38.1 nm, respectively. Correspondingly, N_2 adsorption–desorption measurements indicated that the BET specific surface areas of new $LaCoO_3$ after calcination at 120, 500, and 800 °C were 77.9, 56.1, and 32.7 m^2/g, respectively. These data confirm the relationship that the greater is the particle size, the smaller is the specific surface area due to the sintering of perovskite crystals as the calcination temperature of $LaCoO_3$ increases. It can also be noticed from Figs. 1 and 2 that the perovskite structure of new $LaCoO_3$ remains plausibly unchanged after calcination at 800 °C, because only a small extra peak at 36.9° for trace amounts of Co_3O_4 is observed, and the perovskite structure of conventional $LaCoO_3$ is retained perfectly stable after calcination at 950 °C.

The IR spectrum of conventional $LaCoO_3$ exhibited a set of notable bands at 667 w, 594 s, 559 sh, 419 m, 337 m, and 178 m cm^{-1} as shown in Fig. 3, which are in agreement with those reported in the literature.[26] In contrast, an IR spectrum of new

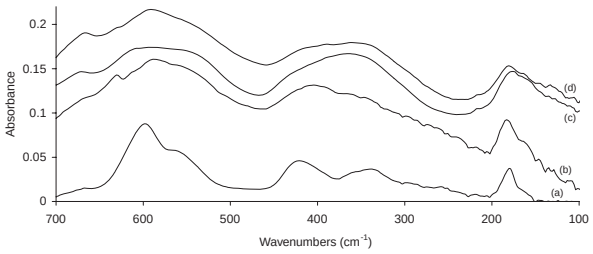

Fig. 3. IR spectra of (a) conventional $LaCoO_3$; (b) new $LaCoO_3$ (3 m^2/g); (c) new $LaCoO_3$ (45 m^2/g); (d) new $LaCoO_3$ (35 m^2/g).

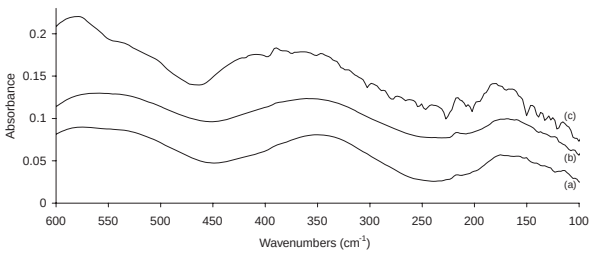

Fig. 4. IR spectra of new $LaCoO_3$ calcined at (a) 120 °C (77.9 m^2/g); (b) 500 °C; (c) 800 °C.

$LaCoO_3$ presented rather broad and ill-resolved bands. Without adding any grinding additives, $LaCoO_3$ achieved by mechanical grinding, which displayed a specific surface area of 3 m^2/g, resulted in a quite similar spectrum to that of conventional $LaCoO_3$ with regular broadening of all the bands (Fig. 3(b)). After continued milling treatments in the presence of NaCl and ZnO as additives, the specific surface areas attained to 45 and 35 m^2/g and the spectral bands further broadened in the meantime (Figs. 3(c) and 3(d)). The 594 and 559 cm^{-1} bands were superimposed into a large one and the 419 and 337 cm^{-1} bands into another large one. By virtue of the perfect XRD spectrum of $LaCoO_3$ prepared by reactive grinding with ZnO, the observed broad IR bands can still reasonably be assigned to the structural vibrations of the $LaCoO_3$ perovskite in spite of the bad spectral resolution. Furthermore, calcination treatments of such a sample at higher temperatures rarely altered the IR spectral shape, as shown in Fig. 4. After calcination at 800 °C, the appearance of a weak additional band at 578 cm^{-1} and a shift of the 357 cm^{-1} band to 380 cm^{-1} are attributed to the formation of trace amounts of Co_3O_4 and La_2O_3, referring to the IR spectra of Co_3O_4 and La_2O_3 presented in Fig. 6. This is consistent with the XRD result. The IR spectral evolution in Fig. 4 implies that the IR band broadening of new $LaCoO_3$ is independent of the particle size of $LaCoO_3$. Such an IR spectral difference between new and conventional $LaCoO_3$ is not understood. The unexpected IR spectral shape of new $LaCoO_3$ may tentatively be attributed to a considerable amount of oxygen defects in the bulk of $LaCoO_3$. The high oxygen defect density of new $LaCo_{1-x}Fe_xO_3$ perovskites has been assumed by us according to their high catalytic activity for the oxidation of volatile organic compounds.[10]

New $LaCoO_3$ showed a different TPR profile than that of conventional $LaCoO_3$ under identical experimental conditions, as shown in Fig. 5. The TPR behavior of the latter is consistent with that reported in the literature,[8,27,28] two principal peaks

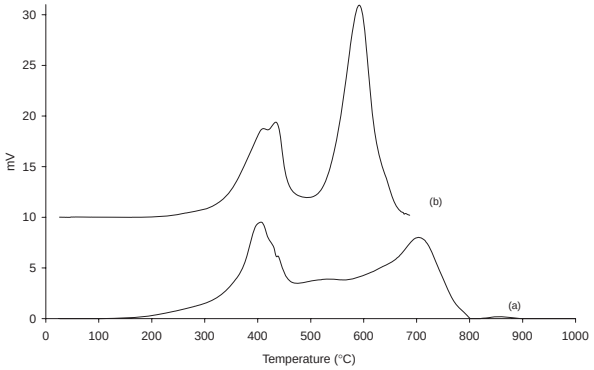

Fig. 5. TPR profiles of (a) new $LaCoO_3$ calcined at 500 °C (56.1 m^2/g); (b) conventional $LaCoO_3$ under 5% H_2/Ar at 10 °C/min.

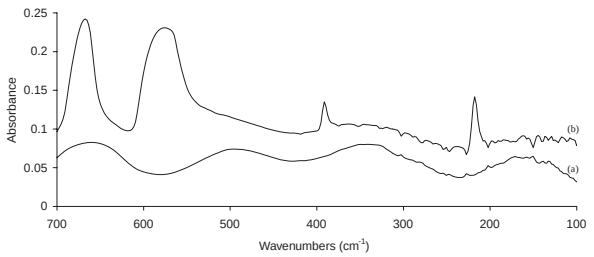

Fig. 6. IR spectra of (a) La_2O_3; (b) Co_3O_4.

appearing at 414 and 595 °C and the second one being nearly triple the first one in area. The TPR profile of the former calcined at 500 °C presented four visible peaks at 411, 530, 709, and 860 °C, suggesting that there would exist at least four types of Co^{3+} sites in the crystallite structure of new $LaCoO_3$. The first peak was similar to that in the case of conventional $LaCoO_3$. The subsequent H_2 consumptions became irregular and the last principal peak was observed at 709 °C in equivalent area to the first one, unlike the case of conventional $LaCoO_3$. Evidently, the reduction chemistry of new $LaCoO_3$ is complex. The temperature (800 °C) at which new $LaCoO_3$ is roughly fully reduced is 113 °C higher than the corresponding one (687 °C) for conventional $LaCoO_3$. At 640 °C, the reduction of conventional $LaCoO_3$ was nearly full while the reduction percent of new $LaCoO_3$ reached only 67. This clearly accounts for the fact that new $LaCoO_3$ is more difficult to reduce than conventional $LaCoO_3$. The emergence of multiple TPR peaks for $LaCoO_3$ may be due to a distortion of the cubic perovskite lattice and the oxygen defect, which would possibly create distinct Co^{3+} environments and reducibilities in the crystallite structure of $LaCoO_3$. Quantitative analysis indicated that the reduction process

$$2LaCoO_3 + 3H_2 \rightarrow La_2O_3 + 2Co^0 + 3H_2O, \quad (1)$$

was completed on both new and conventional $LaCoO_3$ after TPR. The different reducibilities of Co^{3+} in new and conventional $LaCoO_3$ are related to the distinct natures of Co^{3+} sites.

In order to shed light on the effects of the physical properties of $LaCoO_3$ on its chemical properties and structural stability, we investigated the redox behavior of new and conventional $LaCoO_3$ and explored their structural stability in 5% H_2/Ar. For selecting appropriate pretreatment conditions and experi-

Table 2. Principal TPR Peak Maxima of New $LaCoO_3$[a] as a Function of Calcination Temperature

Principal peak	Calcination temperature/°C			
	120	250	500	800
1	361	368	389	475
2	384	700	716	756

a) With a specific surface area of 77.9 m^2/g after calcination at 120 °C.

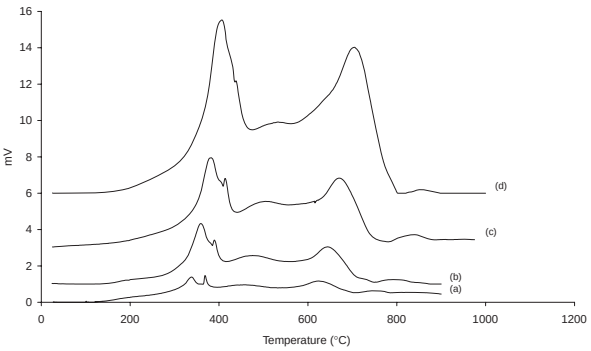

Fig. 7. TPR profiles under 5% H_2/Ar of new $LaCoO_3$ calcined at 500 °C (56.1 m^2/g) at (a) 1 °C/min; (b) 3 °C/min; (c) 5 °C/min; (d) 10 °C/min.

mental parameters, the TPR condition tests were conducted on new $LaCoO_3$ samples as functions of the calcination temperature and the heating rate under 5% H_2/Ar. As can be seen in Table 2, the principal TPR peaks shifted obviously to higher reduction temperatures at a heating rate of 10 °C/min as the calcination temperature increased. The first peak maximum went from 361 to 475 °C and the second one from 684 to 756 °C, while the calcination temperature was varied from 120 to 800 °C. This demonstrates that increasing the calcination temperature of $LaCoO_3$ leads to an increase in the reduction temperature of $LaCoO_3$, which can be explained by the particle size effect on the reduction of $LaCoO_3$. According to Fig. 7, the TPR peaks shifted to lower reduction temperatures as the heating rate decreased on new $LaCoO_3$ samples calcined at 500 °C. This trend is expected. The peak maxima at 410 and 709 °C shifted to 342 and 631 °C, respectively, while the heating rate was decreased from 10 to 1 °C/min. We reckon that the calcination temperature of 500 °C is proper for the pretreatment of new $LaCoO_3$ and comparable to that (600 °C) used for conventional $LaCoO_3$. Also, the heating rate of 10 °C/min is the most practical for TPR experiments, considering both the reduction temperature and the reduction time factors.

Figures 8, 9, 10, and 11 show the redox behaviors of new $LaCoO_3$ calcined at 500 °C and conventional $LaCoO_3$. In the case of new $LaCoO_3$, programmed reduction at 10 °C/min from 23 to 550 °C followed by 2 h of isothermic reduction at 550 °C produced a H_2 consumption curve as seen in Fig. 8(a), whose integral area corresponded to a reduction degree of 81% on $LaCoO_3$. After 1 h of re-oxidation at 500 °C under 20% O_2/He, the resulting sample was subjected to TPR from 23 to 900 °C at 10 °C/min. A similar TPR profile to that of new $LaCoO_3$ was observed (Fig. 9(a)), suggesting

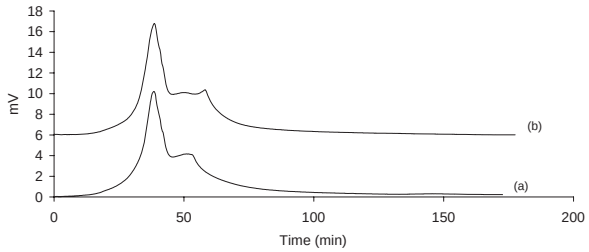

Fig. 8. TPR profiles under 5% H_2/Ar of new $LaCoO_3$ calcined at 500 °C (56.1 m^2/g) at (a) 10 °C/min from 23 to 550 °C followed by 2 h of isothermic heating at 550 °C; (b) 10 °C/min from 23 to 600 °C followed by 2 h of isothermic heating at 600 °C.

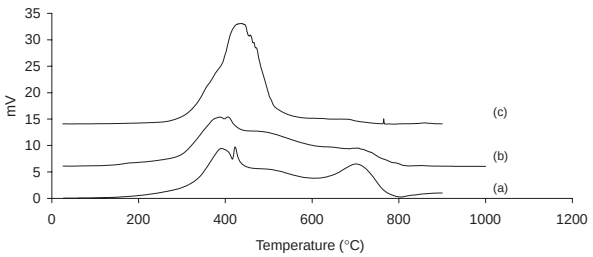

Fig. 9. TPR profiles under 5% H_2/Ar at 10 °C/min of (a) the sample in Fig. 8(a) following 1 h of re-oxidation at 500 °C under 20% O_2/He; (b) the sample in Fig. 8(b) following 1 h of re-oxidation at 500 °C under 20% O_2/He; (c) Co_3O_4/La_2O_3 (Co:La = 1:1 atomic Ratio).

that the sample prior to TPR had the nature of the $LaCoO_3$ perovskite. It can be inferred that new $LaCoO_3$ is reversibly reduced at below 550 °C under 5% H_2/Ar and that the perovskite lattice structure of new $LaCoO_3$ is still retained after reduction under such conditions. When programmed reduction at 10 °C/min from 23 to 600 °C followed by 2 h of isothermic reduction at 600 °C was processed, another H_2 consumption curve was obtained (Fig. 8(b)), whose integral area gave a reduction degree of 85% on $LaCoO_3$. Following 1 h of re-oxidation at 500 °C under 20% O_2/He, the TPR profile of the resulting sample (Fig. 9(b)) deviated from that of new $LaCoO_3$. This illustrates that the perovskite lattice structure of new $LaCoO_3$ is destroyed after reduction at 600 °C and that the reduction of new $LaCoO_3$ at roughly above 600 °C under 5% H_2/Ar is irreversible.

In a series of experiments, we discovered that increasing the calcination temperature of $LaCoO_3$ can enhance the stability of the $LaCoO_3$ perovskite under reducing conditions. For new $LaCoO_3$ calcined at 800 °C, the perovskite lattice structure is maintained stable after reduction at 600 °C under 5% H_2/Ar.

In the case of conventional $LaCoO_3$, programmed reduction at 10 °C/min from 23 to 450 °C followed by 2 h of isothermic reduction at 450 °C resulted in a H_2 consumption curve as seen in Fig. 10(a), whose integral area corresponded to a reduction degree of 48% on $LaCoO_3$. After 1 h of re-oxidation of the resulting sample at 500 °C, an identical TPR profile with that of conventional $LaCoO_3$ appeared (Fig. 11(a)). Programmed reduction at 10 °C/min from 23 to 500 °C followed by 2 h of isothermic reduction at 500 °C led to another H_2 consumption curve (Fig. 10(b)), whose integral area gave a reduction degree

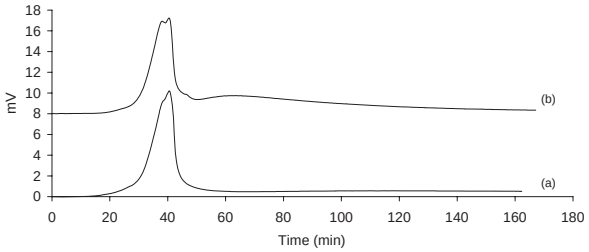

Fig. 10. TPR profiles of conventional $LaCoO_3$ under 5% H_2/Ar at (a) 10 °C/min from 23 to 450 °C followed by 2 h of isothermic heating at 450 °C; (b) 10 °C/min from 23 to 500 °C followed by 2 h of isothermic heating at 500 °C.

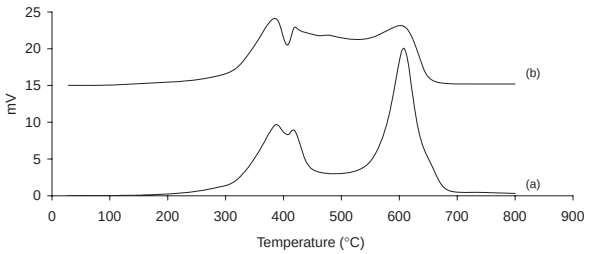

Fig. 11. TPR profiles under 5% H_2/Ar at 10 °C/min of (a) the sample in Fig. 10(a) following 1 h of re-oxidation at 500 °C under 20% O_2/He; (b) the sample in Fig. 10(b) following 1 h of re-oxidation at 500 °C under 20% O_2/He.

of 70% on $LaCoO_3$. However, the sample could not have the TPR profile of conventional $LaCoO_3$ as shown in Fig. 11(b), following 1 h of re-oxidation at 500 °C. The results demonstrate that only at roughly below 450 °C can the perovskite lattice structure of conventional $LaCoO_3$ maintain its stability under 5% H_2/Ar.

These TPR results are evidenced by XRD and IR data. Figures 12 and 13 show the XRD evolution during the redox treatment process of new and conventional $LaCoO_3$. After the reduction of new $LaCoO_3$ at 400 and 500 °C under 5% H_2/Ar, following the same procedure as mentioned above, the resulting samples gave the same XRD pattern as that of $LaCoO_3$ with lower diffraction intensities. When the reduction temperature was raised to 550 °C, a slight downward shift of peaks of $LaCoO_3$ occurred together with the appearance of a weak peak at 44.5°. The latter peak is assigned to Co^0. Re-oxidation of the reduced sample at 500 °C restored the peak positions of $LaCoO_3$ and slightly increased the peak intensity. The simultaneous appearance of a weak peak at 37.1° is attributed to the formation of a trace amount of Co_3O_4 by the oxidation of a trace amount of Co^0. The XRD observations turn out to show that the perovskite lattice structure of new $LaCoO_3$ essentially remains unchanged, having experienced reduction at below 550 °C under 5% H_2/Ar. Once the reduction temperature reached 600 °C, all peaks of $LaCoO_3$ almost disappeared along with the concomitant appearance of a peak of Co^0 at 44.4°. Subsequent re-oxidation at 500 °C could result in no peak except that of Co_3O_4 at 37.1°. It is thus clear that the reduction at above 600 °C under 5% H_2/Ar caused a collapse of the perovskite lattice structure of new $LaCoO_3$ via the sintering of cobalt atoms.

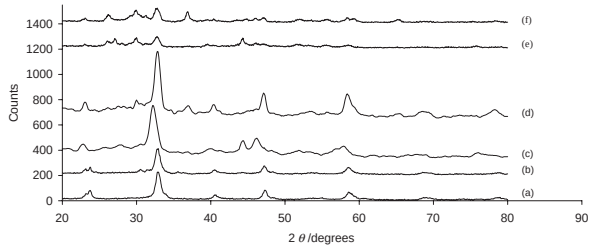

Fig. 12. XRD patterns for new $LaCoO_3$ calcined at 500 °C (56.1 m^2/g) (a) after TPR under 5% H_2/Ar at 10 °C/min from 23 to 400 °C followed by 2 h of isothermic heating at 400 °C; (b) after TPR under 5% H_2/Ar at 10 °C/min from 23 to 500 °C followed by 2 h of isothermic heating at 500 °C; (c) after TPR under 5% H_2/Ar at 10 °C/min from 23 to 550 °C followed by 2 h of isothermic heating at 550 °C; (d) after 1 h of re-oxidation at 500 °C under 20% O_2/He following (c); (e) after TPR under 5% H_2/Ar at 10 °C/min from 23 to 600 °C followed by 2 h of isothermic heating at 600 °C; (f) after 1 h of re-oxidation at 500 °C under 20% O_2/He following (e).

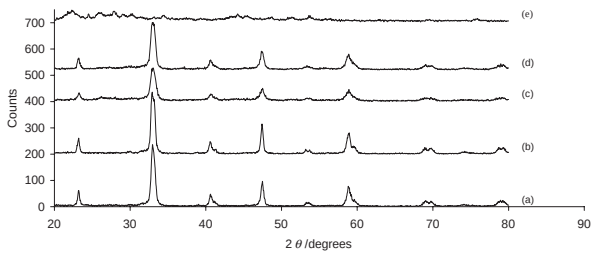

Fig. 13. XRD patterns for conventional $LaCoO_3$ (a) after TPR under 5% H_2/Ar at 10 °C/min from 23 to 400 °C followed by 2 h of isothermic heating at 400 °C; (b) after 1 h of re-oxidation at 500 °C under 20% O_2/He following (a); (c) after TPR under 5% H_2/Ar at 10 °C/min from 23 to 450 °C followed by 2 h of isothermic heating at 450 °C; (d) after 1 h of re-oxidation at 500 °C under 20% O_2/He following (c); (e) after TPR under 5% H_2/Ar at 10 °C/min from 23 to 500 °C followed by 2 h of isothermic heating at 500 °C.

In contrast, the XRD spectrum of conventional $LaCoO_3$ was observed only after reduction at below 450 °C under 5% H_2/Ar, as shown in Fig. 13. Re-oxidation at 500 °C did not modify the XRD pattern of $LaCoO_3$ except that it enhanced the diffraction intensity for reduction at 450 °C. Reduction at above 500 °C resulted in the disappearance of all the peaks of $LaCoO_3$ and the appearance of a peak of Co^0 at 44.3°. It is evident that the perovskite lattice structure of conventional $LaCoO_3$ is less stable than that of new $LaCoO_3$ under identical reducing conditions.

Figures 14 and 15 show the IR spectral evolution during the redox treatment processes of new and conventional $LaCoO_3$. After the reduction of new $LaCoO_3$ at 500 °C under 5% H_2/Ar according to the same manner as mentioned above, the resulting sample displayed three broad bands at 546, 370, and 166 cm^{-1} (Fig. 14(a)). This spectrum resembles that for new $LaCoO_3$ calcined at 500 °C (Fig. 4(b)) with a significant shift of the 357 cm^{-1} band to 370 cm^{-1}, indicating that the reduced

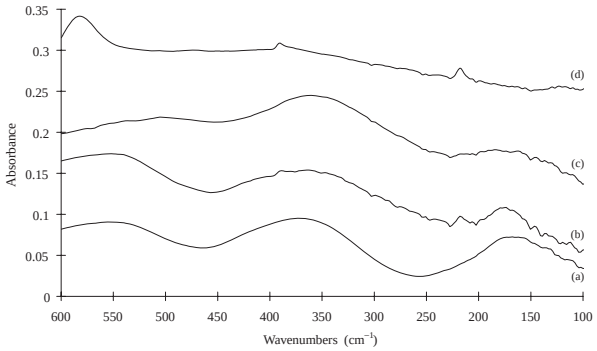

Fig. 14. IR spectra for new $LaCoO_3$ calcined at 500 °C (56.1 m^2/g) (a) after TPR under 5% H_2/Ar at 10 °C/min from 23 to 500 °C followed by 2 h of isothermic heating at 500 °C; (b) after 1 h of re-oxidation at 500 °C under 20% O_2/He following (a); (c) after TPR under 5% H_2/Ar at 10 °C/min from 23 to 600 °C followed by 2 h of isothermic heating at 600 °C; (d) after 1 h of re-oxidation at 500 °C under 20% O_2/He following (c).

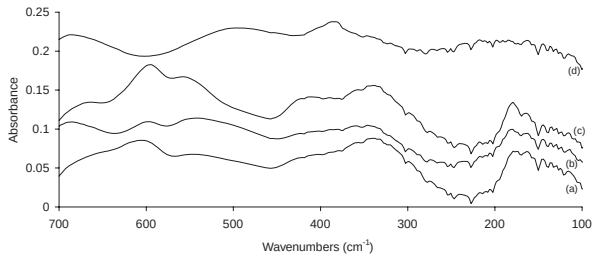

Fig. 15. IR spectra for conventional $LaCoO_3$ (a) after TPR under 5% H_2/Ar at 10 °C/min from 23 to 400 °C followed by 2 h of isothermic heating at 400 °C; (b) after 2 weeks of re-oxidation at 23 °C under 20% O_2/He following (a); (c) after 1 h of re-oxidation at 500 °C under 20% O_2/He following (b); (d) after TPR under 5% H_2/Ar at 10 °C/min from 23 to 500 °C followed by 2 h of isothermic heating at 500 °C.

sample contained the remaining $LaCoO_3$ together with a new component. Apparently, the perovskite lattice structure in the reduced sample remained, since no additional bands such as those for La_2O_3 were observed. After the re-oxidation of the reduced sample at 500 °C, there was little modification in spectral pattern as shown in Fig. 14(b) relative to Fig. 14(a), except for a retro-shift of the 370 cm^{-1} band to 360 cm^{-1}. This seems to show that the new component was re-oxidized to $LaCoO_3$. Thus, the reduced sample is assumed to be in the form of $LaCoO_{3-x}$. However, reduction at 600 °C led to the appearance of another set of bands at 501, 359, and 168 cm^{-1} (Fig. 14(c)) instead of the bands at 546, 370, and 166 cm^{-1} for new $LaCoO_3$. These three new bands are similar to those characteristic of La_2O_3 presented in Fig. 6(a). Since the vibrational spectral features of chemical bonds in the perovskite lattice no longer emerge, it is concluded that the $LaCoO_3$ perovskite was already disintegrated into Co^0/La_2O_3. Subsequent re-oxidation at 500 °C produced a notable band at 579 cm^{-1} (Fig. 14(d)), which corresponded to one of the vibrational modes of the Co–O bond in Co_3O_4 (Fig. 6(b)). This confirms that the perovskite lattice structure of new $LaCoO_3$ was destroyed with the formation of Co^0/La_2O_3 after reduction at 600 °C under 5% H_2/Ar.

In the case of conventional $LaCoO_3$, reduction at 400 °C gave rise to six broad bands at 654 sh, 602, 540, 405 sh, 339, and 175 cm^{-1}, as can be seen in Fig. 15(a). The band positions are compatible to those of conventional $LaCoO_3$. However, the intensity of the bands at 602, 540, and 405 cm^{-1} is relatively low with respect to that of the bands at 594, 559, and 419 cm^{-1} in the spectrum of conventional $LaCoO_3$ (Fig. 3(a)). This suggests that the reduced sample consists of the remaining $LaCoO_3$ and a new component. The latter does not belong to Co^0/La_2O_3, since the bands for La_2O_3 do not appear in Fig. 15(a). Extended exposure of the reduced sample to air at 23 °C brought about a slight increase in the spectral intensity. This accounts for the fact that the new component is hardly converted back to $LaCoO_3$ by oxidation in air at ambient temperature. Upon re-oxidation at 500 °C, the relative intensity of the bands at 594, 553, and 411 cm^{-1} to the bands at 337 and 177 cm^{-1} increased largely as shown in Fig. 15(c). The obtained spectrum coincides with that of conventional $LaCoO_3$. The results demonstrate that the perovskite lattice structure of the new component is still retained and that $LaCoO_3$ can be effectively regenerated from this component by oxidation at 500 °C. The reduced sample is believed to have a formula like $LaCoO_{3-x}$. When the reduction temperature was raised to 500 °C, the observed spectrum resembled that of La_2O_3, as presented in Fig. 15(d). This implied that $LaCoO_3$ is already transformed to Co^0/La_2O_3 under such reducing conditions.

It is obvious that the results in studies of the redox chemistry of $LaCoO_3$ by TPR, XRD, and IR are fairly consistent.

It appears apparent from the present work that the stability of the $LaCoO_3$ perovskite structure under a reducing atmosphere is dependent on the redox behavior of $LaCoO_3$ itself. The higher the temperature for completing the reductive reaction of $LaCoO_3$ in Eq. 1, the more stable the $LaCoO_3$ perovskite structure under a reducing atmosphere. Since the temperature at which new $LaCoO_3$ is completely reduced is markedly higher than that for conventional $LaCoO_3$, the former displays a significantly higher destruction temperature of the perovskite structure under a reducing atmosphere than the latter. As the reduction temperature of $LaCoO_3$ increases with increasing calcination temperature of $LaCoO_3$, the stability of the $LaCoO_3$ perovskite structure under a reducing atmosphere tends to be reinforced by increasing the calcination temperature. The good stability of the perovskite structure under reducing conditions is of significant importance for perovskite-type oxide catalyzed hydrogenation reactions. As long as the perovskite structure remains, the cobalt may be present in the form of highly dispersed Co^0 in the lattice. It is expected that such perovskite catalysts are quite effective for hydrogenation. Furthermore, La^{3+} is known as a promoter of Co/SiO_2 for CO hydrogenation.[29] It may be imagined that $LaCoO_3$ would be a competitive hydrogenation catalyst precursor.

Conclusion

We have compared the XRD spectra, IR spectra, and TPR profiles of new and conventional $LaCoO_3$. These characterization and test results reveal the differences in the physical prop-

erty and surface chemistry between them. Although they both have the same perovskite X-ray structure, new $LaCoO_3$ possesses a smaller particle size and a greater specific surface area. Moreover, new $LaCoO_3$ is suggested to have many oxygen defects. Compared to conventional $LaCoO_3$, new $LaCoO_3$ is obviously difficult to reduce to Co^0/La_2O_3.

We have also studied the stability of the $LaCoO_3$ perovskite structure under reducing conditions by observing the redox behavior of $LaCoO_3$. The reducibility of Co^{3+} in $LaCoO_3$ determines the stability of the perovskite lattice structure. Due to the higher temperature required for completely reducing new $LaCoO_3$, the perovskite lattice structure of new $LaCoO_3$ is more stable than that of conventional $LaCoO_3$.

This research was supported by the Natural Sciences and Engineering Research Council of Canada (NSERC) with a strategic grant.

References

1 L. G. Tejuca, J. L. G. Fierro, and J. M. D. Tascn, *Adv. Catal.*, **36**, 237 (1989).

2 L. G. Tejuca and J. L. G. Fierro, "Properties and Applications of Perovskite-type Oxides," Marcel Dekker, New York (1992).

3 M. Skoglundh, L. Lwendhal, K. Jansson, L. Dahland, and M. Nygren, *Appl. Catal., B*, **3**, 259 (1994).

4 M. Cal, R. Oukac, and G. Marcelin, *Ind. Eng. Chem. Res.*, **33**, 2930 (1994).

5 J. Wang, H. Yasuda, K. Inumaru, and M. Misono, *Bull. Chem. Soc. Jpn.*, **68**, 1226 (1995).

6 H. G. Lintz and K. Wittstock, *Catal. Today*, **29**, 457 (1996).

7 Z. Zhao, X. Yang, and Y. Wu, *Appl. Catal., B*, **8**, 281 (1996).

8 R. Lago, G. Bini, M. A. Pea, and J. L. G. Fierro, *J. Catal.*, **167**, 198 (1997).

9 M. A. Pea and J. L. G. Fierro, *Chem. Rev.*, **101**, 1981 (2001).

10 V. Szabo, M. Bassir, A. van Neste, and S. Kaliaguine, *Appl. Catal., B*, **37**, 175 (2002).

11 S. V. Nguyen, V. Szabo, D. Trong On, and S. Kaliaguine, *Micropor. Mesopor. Mater.*, **54**, 51 (2002).

12 N. K. Labhsetwar, A. Watanabe, and T. Mitsuhashi, *Appl. Catal., B*, **40**, 21 (2003).

13 R. J. H. Voorhoeve, J. P. Remeika, P. E. Freeland, and B. T. Mathias, *Science*, **177**, 353 (1972).

14 H. Arai, T. Yamada, K. Eguchi, and T. Seiyama, *Appl. Catal.*, **26**, 265 (1986).

15 J. O. Petunchi, J. L. Nicastro, and E. A. Lombardo, *J. Chem. Soc., Chem. Commun.*, **1980**, 467.

16 K. Ichimura, Y. Inoue, and I. Yasumori, *Bull. Chem. Soc. Jpn.*, **53**, 3044 (1980).

17 K. Ichimura, Y. Inoue, and I. Yasumori, *Bull. Chem. Soc. Jpn.*, **54**, 1787 (1981).

18 P. R. Watson and G. A. Somorjai, *J. Catal.*, **74**, 282 (1982).

19 J. N. Nudel, B. S. Umansky, R. O. Piagentini, and E. A. Lombardo, *J. Catal.*, **89**, 362 (1984).

20 M. A. Ulla, R. A. Migone, J. O. Petunchi, and E. A. Lombardo, *J. Catal.*, **105**, 107 (1987).

21 H. J. Gysling, J. R. Monnier, and G. Apai, *J. Catal.*, **103**, 407 (1987).

22 C. Marcilly, P. Courty, and B. Delmon, *J. Am. Ceram. Sci.*, **53**, 56 (1970).

23 D. J. Anderton and F. R. Sale, *Powder. Metall.*, **22**, 14 (1979).

24 S. Kaliaguine and A. van Neste, U.S. Patent 6017504 (2000).

25 S. Kaliaguine, A. van Neste, V. Szabo, J. E. Gallot, M. Bassir, and R. Muzychuk, *Appl. Catal., A*, **209**, 345 (2001).

26 M. Couzi and P. V. Huong, *J. Chim. Phys.*, **69**, 1339 (1972).

27 M. Crespin and W. K. Hall, *J. Catal.*, **69**, 359 (1981).

28 F. Ma, Y. Chen, and H. Lou, *React. Kinet. Catal. Lett.*, **31**, 47 (1986).

29 G. J. Haddad, B. Chen, and J. G. Goodwin, Jr., *J. Catal.*, **161**, 274 (1996).